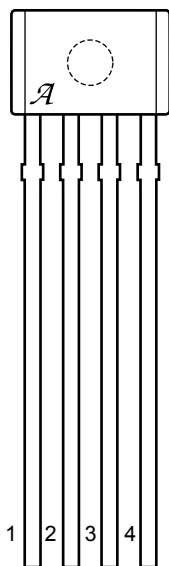


# A1421, A1422, A1423

## High Accuracy Analog Speed Sensor with Integrated Filter Capacitor

Package K, 4-pin SIP



1. VCC
2. VOUT
3. Test pin, tie to GND
4. GND

### ABSOLUTE MAXIMUM RATINGS

Supply Voltage, $V_{CC}$ .....	28 V
Reverse-Supply Voltage, $V_{RCC}$ .....	-18 V
Output Current, $I_{OUT}$ .....	25 mA
Reverse-Output Current, $I_{ROUT}$ .....	-50 mA
Reverse-Output Voltage, $V_{ROUT}$ .....	-50 mA
Operating Temperature	
Ambient ( $L$ ), $T_A$ .....	-40°C to 150°C
Maximum Junction, $T_{J(max)}$ .....	165°C
Storage Temperature, $T_S$ .....	-65°C to 170°C

The A1421, A1422, and A1423 are ac-coupled Hall-effect sensors which include monolithic integrated circuits that switch in response to changing differential magnetic fields created by rotating ring magnets, or when coupled with a magnet, by ferrous targets. This family of devices also includes an integrated capacitor, providing the high accuracy of analog sensing without an external filter capacitor. This reduces cost and components, while improving the reliability of the final sensor solution.

The magnetic field changes are sensed by two integrated Hall transducers and then are differentially amplified on the chip. Differential sensing provides immunity to radial vibration, within the device operating air gap range, by rejection of common-mode signal changes. Steady-state system offsets are eliminated using an on-chip differential bandpass filter with integrated capacitor. This filter also provides relative immunity to interference from electromagnetic sources. The device utilizes advanced temperature compensation for the high-pass filter, sensitivity, and Schmitt trigger switchpoints to guarantee optimal operation to low frequencies over a wide range of air gaps and temperatures.

Each device includes a voltage regulator, two Hall transducers, temperature compensating circuitry, a low-level amplifier, bandpass filter, Schmitt trigger, and an output driver. The on-board regulator permits operation with supply voltages from 4.0 to 26.5 V. The output stage can switch 20 mA over the full frequency response range of the sensor, and is compatible with TTL and CMOS logic circuits.

*Continued on next page.*

### Features and Benefits

- Integrated tracking capacitor
- Senses motion of ring magnet or ferrous targets
- Wide operating temperature range
- Operation with frequency of sensed transitions from 20 Hz to 30 kHz
- EMI/ESD-resistant
- Large effective air gaps
- 4.0 to 26.5 V operating range
- Output compatible with both TTL and CMOS logic families
- Reverse battery protection
- Resistant to mechanical and thermal stress

Engineering samples available on a limited basis. Contact your local sales or applications support office for additional information.

The devices in this family differ from each other in their switchpoint specifications and their switching polarity. The A1421 has a small hysteresis and asymmetrical switchpoints, with one switchpoint at the zero-crossing. The A1422 has a small hysteresis and symmetrical switchpoints, both near the zero-crossing. The A1423 offers high vibration immunity, by means of its larger hysteresis, establishing symmetrical switchpoints further from the zero-crossing. The output polarity is shown in the Product Selection Guide table.

This variety of options provides flexibility for achieving solutions for a wide range of applications, including automotive transmission and crankshaft speed sensing.

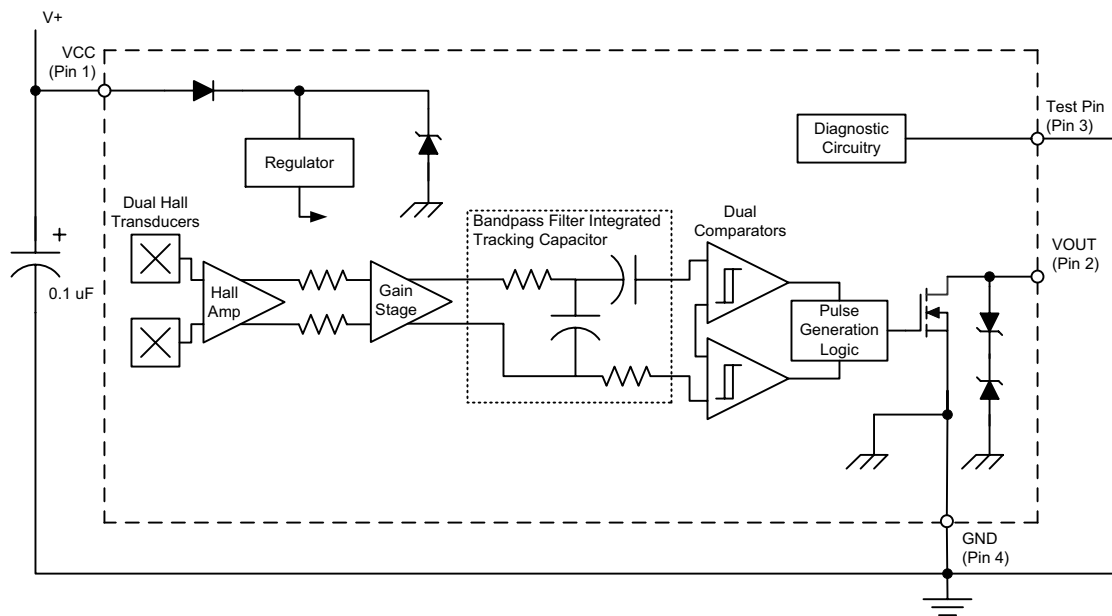
The device package has an operating ambient temperature range  $-40^{\circ}\text{C}$  to  $150^{\circ}\text{C}$  (suffix *L*), and is provided in a 4-pin plastic SIP (part number suffix *K*).

### Product Selection Guide

Use the following complete part numbers when ordering:

Part Number	Output Switching at $B_{\text{DIFF}} = 0$		Switchpoints		Hysteresis	Symmetry		
	$B_{\text{Diff}}$ Increasing	$B_{\text{Diff}}$ Decreasing	$B_{\text{OP}}(\text{typ})$ (G)	$B_{\text{RP}}$ (G)	$B_{\text{Hys}}(\text{typ})$ (G)	$B_{\text{OP}}(\text{max})^{+}$ $B_{\text{RP}}(\text{min})$ (G)	$B_{\text{OP}}(\text{typ})^{+}$ $B_{\text{RP}}(\text{typ})$ (G)	$B_{\text{OP}}(\text{min})^{+}$ $B_{\text{RP}}(\text{max})$ (G)
A1421LK	Low (On) to High (Off)	High (Off) to Low (On)	15	0	15	15	15	7.5
A1422LK	High (Off) to Low (On)	Low (On) to High (Off)	15	-15	30	0	0	0
A1423LK	High (Off) to Low (On)	Low (On) to High (Off)	65	-65	130	0	0	0

### Functional Block Diagram



**OPERATING CHARACTERISTICS** Valid at  $T_A = -40^{\circ}\text{C}$  to  $150^{\circ}\text{C}$ ,  $T_J \leq 165^{\circ}\text{C}$ ; over operational air gap range and  $V_{CC}$  within operating range, unless otherwise noted. Typical operating parameters:  $V_{CC} = 12\text{ V}$  and  $T_A = 25^{\circ}\text{C}$ .

Characteristic	Symbol	Test Conditions	Min.	Typ.	Max.	Units
<b>ELECTRICAL CHARACTERISTICS</b>						
Supply Voltage	$V_{CC}$	Operating; $T_J < T_{J(max)}$	4.0	12.0	26.5	V
Supply Current	$I_{CC}$		–	4.2	7.0	mA
Output Saturation Voltage	$V_{OUT(SAT)}$	$I_{SINK} = 20\text{ mA}$	–	140	400	mV
Output Leakage Current	$I_{OFF}$	$V_{OUT} = 24\text{ V}$ , $B_{diff} = 0$	–	–	5	$\mu\text{A}$
<b>PROTECTION COMPONENT CHARACTERISTICS</b>						
Reverse Supply Current	$I_{RCC}$	$V_{CC} = -18\text{ V}$	–	–	–1	mA
Supply Zener Current	$I_{ZCC}$	$V_{CC} = 28\text{ V}$	–	–	10	mA
Supply Zener Clamp Voltage	$V_{ZCC}$	$I_{CC} = 10\text{ mA}^1$ , $T_A = 25^{\circ}\text{C}$	28	33	37	V
Output Zener Current	$I_{ZOUT}$	$V_{OUT} = 28\text{ V}$	–	–	3	mA
Output Zener Clamp Voltage	$V_{ZOUT}$	$I_{OUT} = 3\text{ mA}$ , $T_A = 25^{\circ}\text{C}$	28	–	–	V
Output Short Circuit Current Limit	$I_{OUT(lim)}$		–	–	50	mA
<b>RESPONSE CHARACTERISTICS</b>						
Power-On State	POS	$t < t_R$	–	High	–	V
Power-On Time <sup>2,6</sup>	$t_{PO}$	$V_{CC} > V_{CC(min)}$	–	4.5	9	ms
Settling Time <sup>3,6</sup>	$t_S$	$f_{Bdiff} \geq 100\text{ Hz}$	0	–	50	ms
Response Time <sup>6</sup>	$t_R$	Equal to $t_{PO} + t_S$ ; $f_{Bdiff} \geq 100\text{ Hz}$	4.5	–	59	ms
Upper Corner Frequency	$f_{cu}$	–3 dB, single pole	30	–	–	kHz
Lower Corner Frequency	$f_{cl}$	–3 dB, single pole	–	–	20	Hz
<b>OUTPUT CHARACTERISTICS</b>						
Output Rise Time <sup>4</sup>	$t_{rise}$	$R_{PU} = 1\text{ k}\Omega$ , $C = 10\text{ pF}$	–	–	200	ns
Output Fall Time	$t_{fall}$	$R_{PU} = 1\text{ k}\Omega$ , $I_{SINK} = 20\text{ mA}$ , $C = 10\text{ pF}$	–	–	200	ns

Continued on next page.

**OPERATING CHARACTERISTICS, continued** Valid at  $T_A = -40^\circ\text{C}$  to  $150^\circ\text{C}$ ,  $T_J \leq 165^\circ\text{C}$ ; over operational air gap range and  $V_{CC}$  within operating range, unless otherwise noted. Typical operating parameters:  $V_{CC} = 12\text{ V}$  and  $T_A = 25^\circ\text{C}$ .

Characteristic	Symbol	Test Conditions	Min.	Typ.	Max.	Units
<b>MAGNETIC CHARACTERISTICS<sup>5</sup></b>						
Operate point	$B_{OP}^6$	1421, $B_{diff}$ increasing, $f_{Bdiff} = 200\text{ Hz}$ , $B_{diff} = 50\text{ Gp-p}$	0.0	15.0	27.5	G
		1422, $B_{diff}$ increasing, $f_{Bdiff} = 200\text{ Hz}$ , $B_{diff} = 50\text{ Gp-p}$	5.0	15.0	35.0	G
		1423, $B_{diff}$ increasing, $f_{Bdiff} = 200\text{ Hz}$ , $B_{diff} = 200\text{ Gp-p}$	10.0	65.0	100.0	G
Release Point	$B_{RP}^6$	1421, $B_{diff}$ decreasing, $f_{Bdiff} = 200\text{ Hz}$ , $B_{diff} = 50\text{ Gp-p}$	-12.5	0.0	7.5	G
		1422, $B_{diff}$ decreasing, $f_{Bdiff} = 200\text{ Hz}$ , $B_{diff} = 50\text{ Gp-p}$	-35.0	-15.0	-5.0	G
		1423, $B_{diff}$ decreasing, $f_{Bdiff} = 200\text{ Hz}$ , $B_{diff} = 200\text{ Gp-p}$	-100.0	-65.0	-10.0	G
Hysteresis	$B_{HYS}^6$	1421, $f_{Bdiff} = 200\text{ Hz}$ , $B_{diff} = 50\text{ Gp-p}$	5	15	35	G
		1422, $f_{Bdiff} = 200\text{ Hz}$ , $B_{diff} = 50\text{ Gp-p}$	-	30	-	G
		1423, $f_{Bdiff} = 200\text{ Hz}$ , $B_{diff} = 200\text{ Gp-p}$	-	130	-	G
Applied Magnetic Field <sup>7</sup>	$B_{diff}$	Differential p-p magnetic field	-	-	1250	G

<sup>1</sup>Equivalent to  $I_{CC(max)} + 3\text{ mA}$ .

<sup>2</sup>Time required to initialize device.

<sup>3</sup>Time required for the output switchpoints to be within specification.

<sup>4</sup>Output Rise Time will be dominated by the RC time constant.

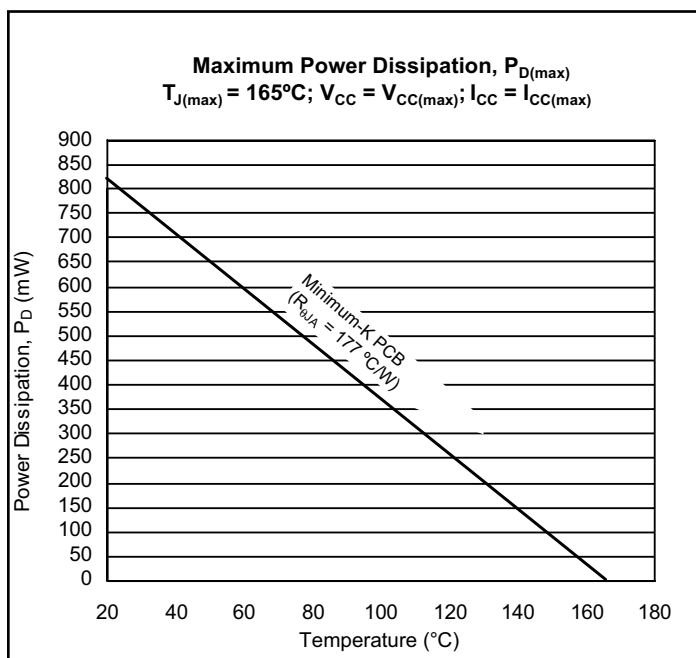
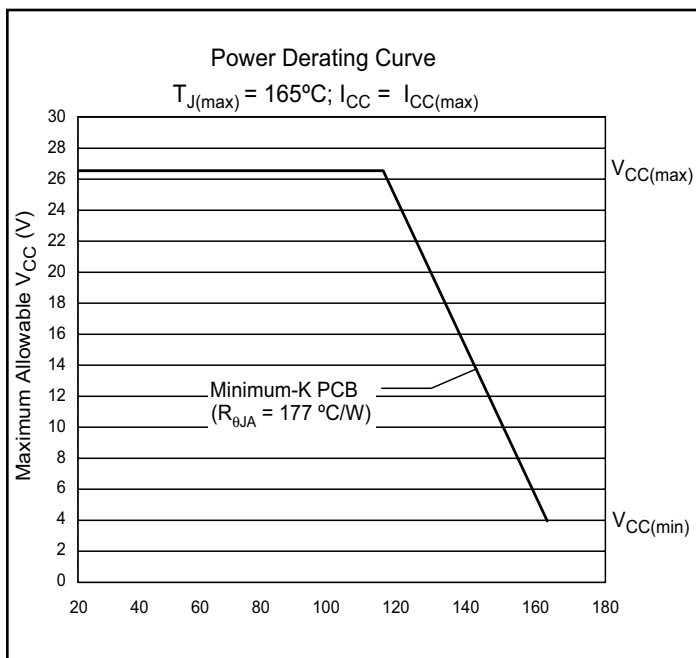
<sup>5</sup>For lower frequencies, the absolute values of  $B_{OP}$ ,  $B_{RP}$ , and  $B_{HYS}$  may decrease due to delay induced by the high-pass filter.

<sup>6</sup> See Definitions of Terms section.

<sup>7</sup> Exceeding the maximum magnetic field may result in compromised absolute accuracy.

### THERMAL CHARACTERISTICS may require derating at maximum conditions, see application information

Characteristic	Symbol	Test Conditions	Min.	Typ.	Max	Units
Package Thermal Resistance	$R_{\theta JA}$	Minimum-K PCB (single-sided with copper limited to solder pads)	177	-	-	°C/W



### Definitions of Terms

The following provide additional information about some of the parameters cited in the Operating Characteristics table. For additional information, visit the Allegro Web site at [www.allegromicro.com](http://www.allegromicro.com).

**Applied Magnetic Field,  $B_{diff}$**  – The differential magnetic flux density which is calculated as the arithmetic difference of the flux densities observed by each of the two Hall elements.

**Output Off Switchpoint (Operate Point),  $B_{OP}$**  – The value of increasing differential magnetic flux density at which the device output switches from low to high (A1421) or high to low (A1422 and A1423).

**Output On Switchpoint (Release Point),  $B_{RP}$**  – The value of decreasing differential magnetic flux density at which the device

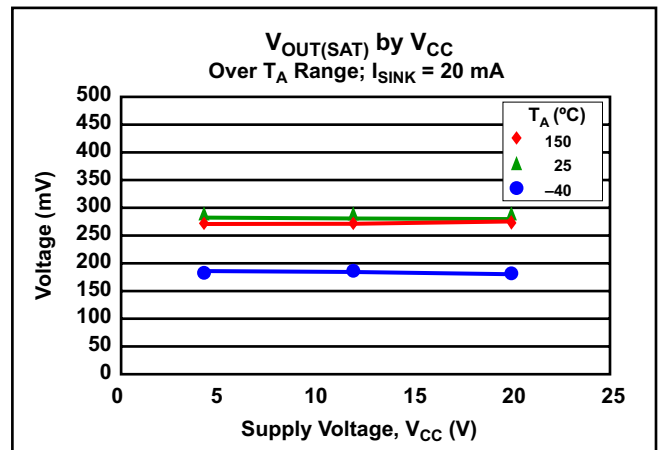
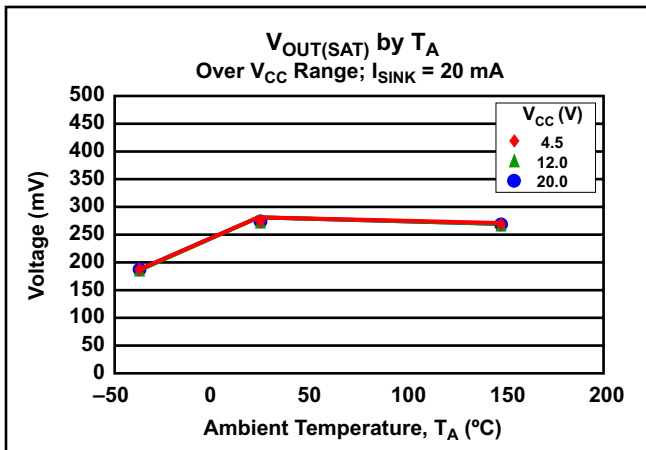
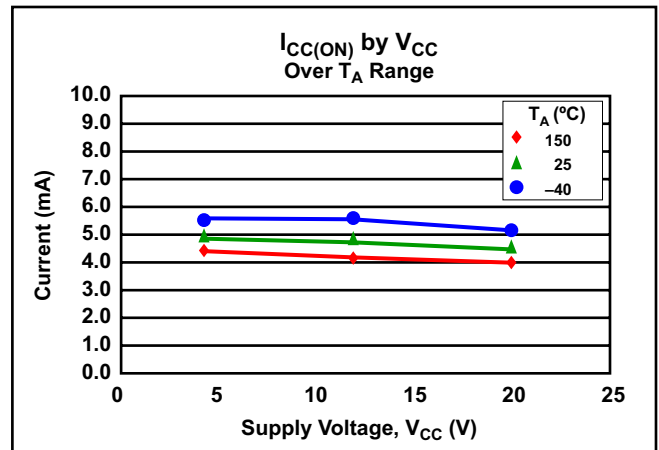
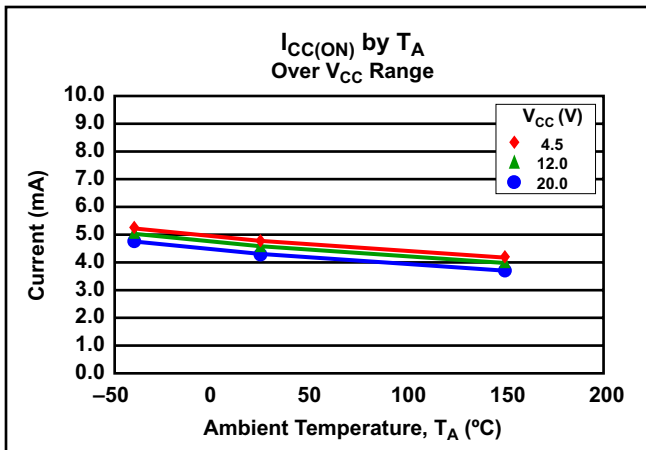
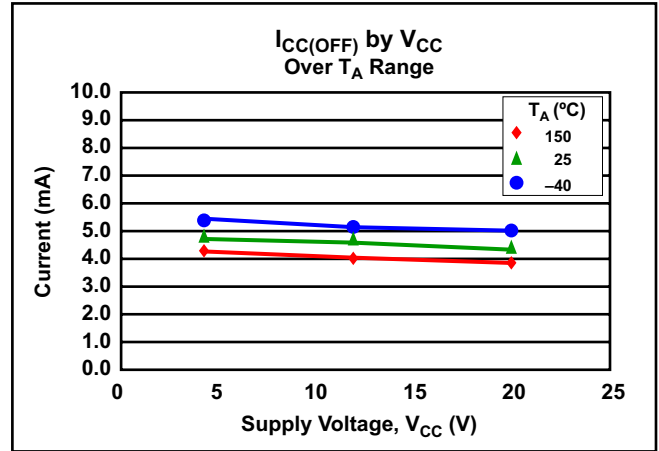
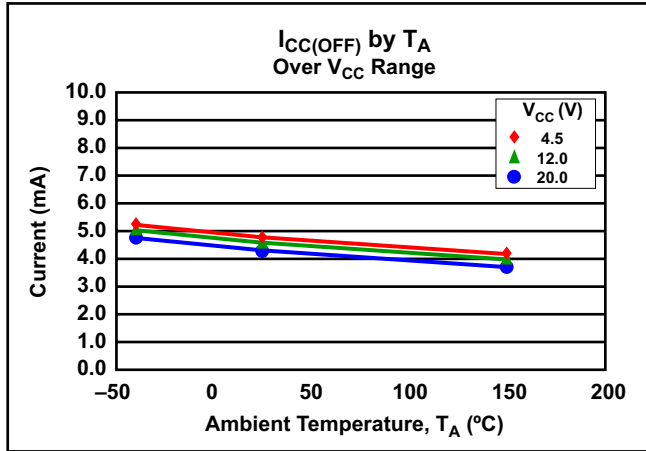
output switches from high to low (A1421) or from low to high (A1422 and A1423).

**Power-On Time,  $t_{PO}$**  – The time needed by the device, after power is applied, to initialize all circuitry necessary for proper operation.

**Settling Time,  $t_S$**  – The time required by the device, after  $t_{PO}$ , and after a valid magnetic signal has been applied, to provide proper output transitions. Settling time is a function of magnetic offset, offset polarity, signal phase, signal frequency, and signal amplitude.

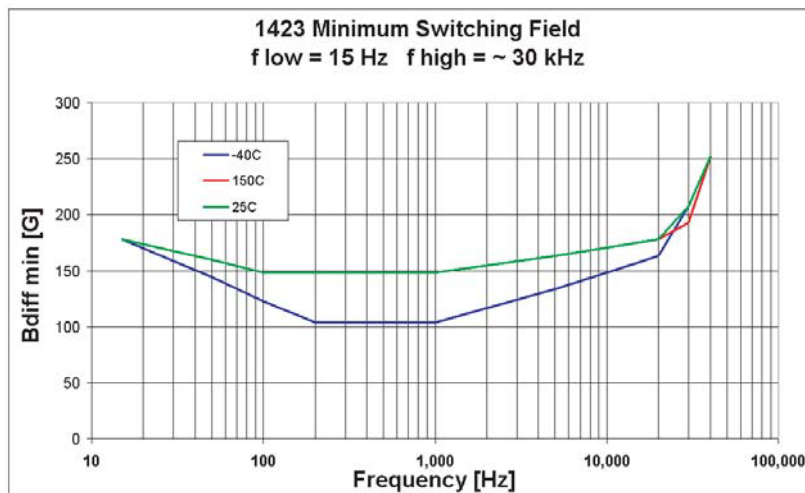
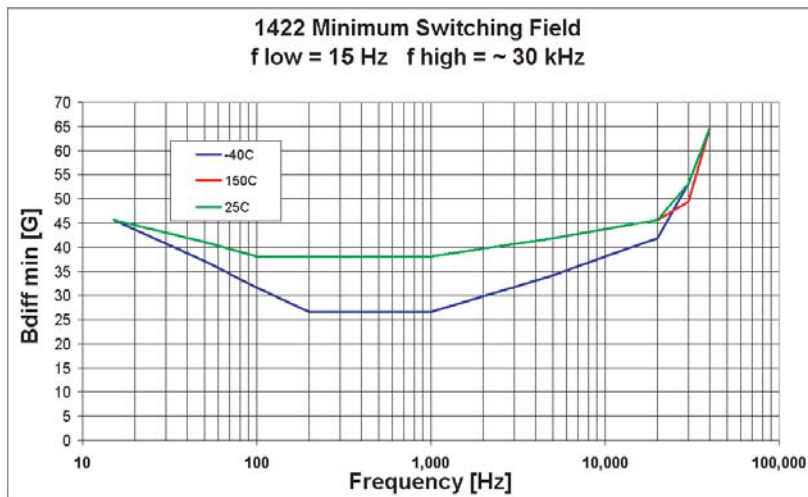
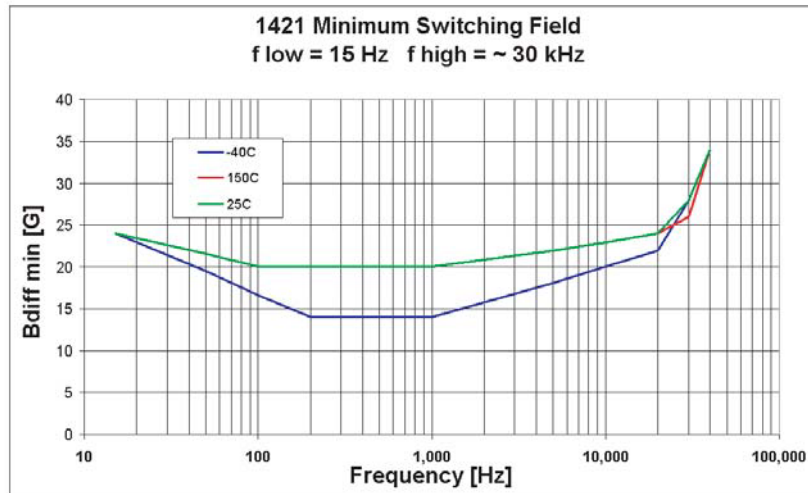
**Response Time,  $t_R$**  – The total time required for generating zero-crossing output transitions after power-up (the sum of power-on time and settling time).

### Empirical Results



Continued on next page.

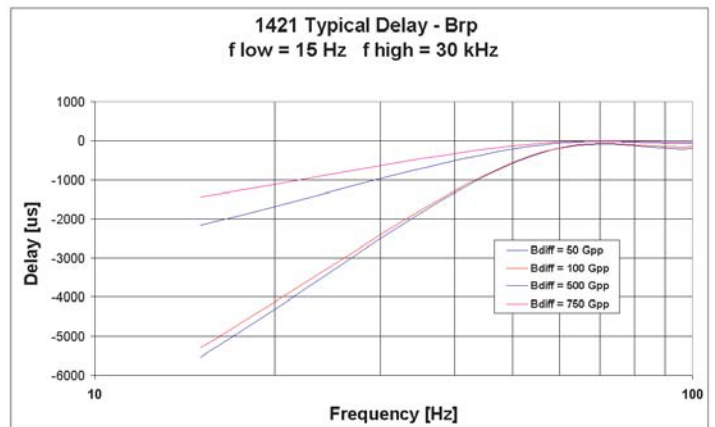
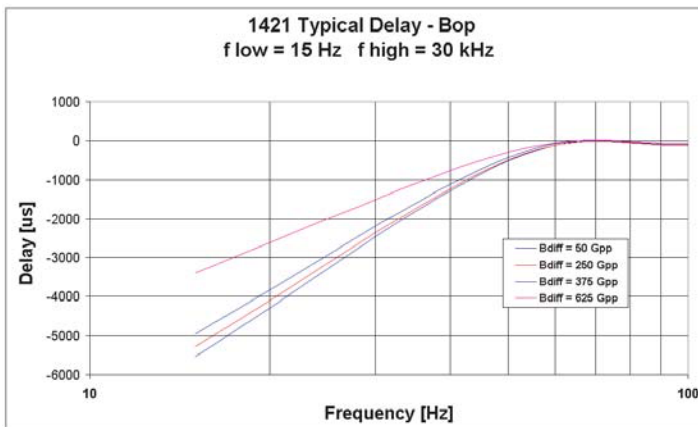
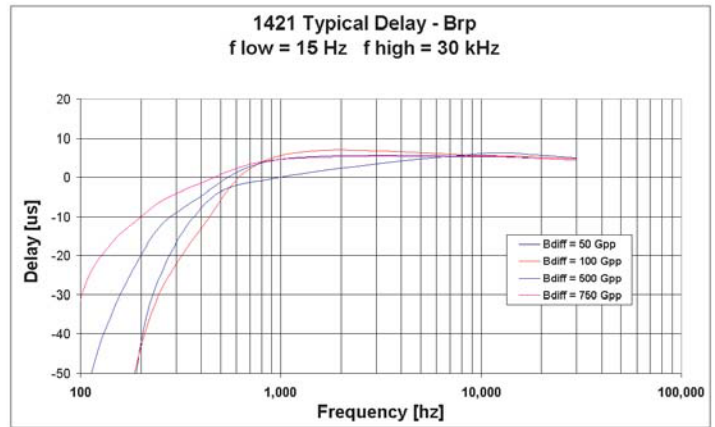
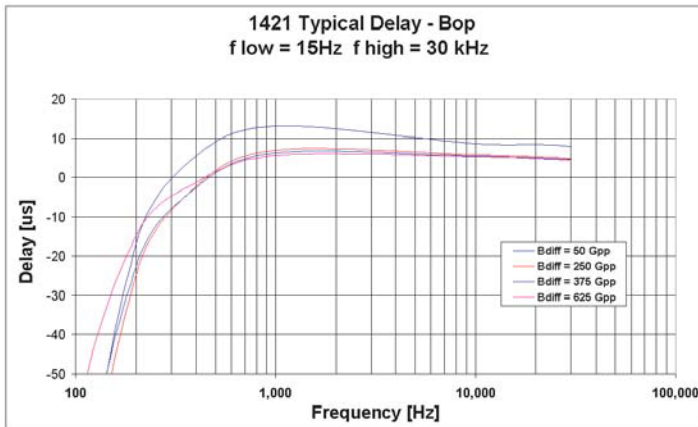
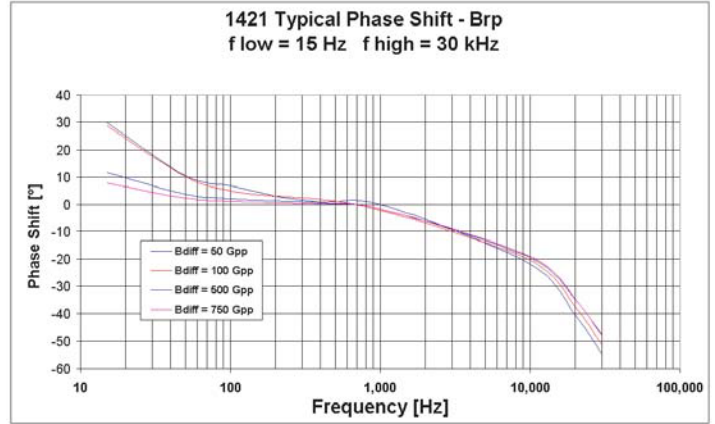
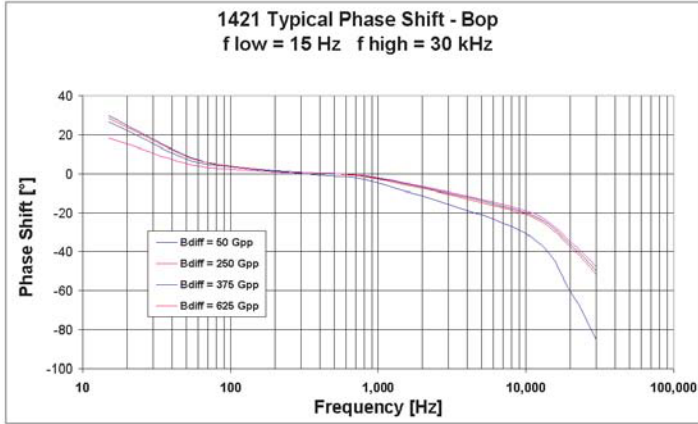
### Simulation Results



Continued on next page.

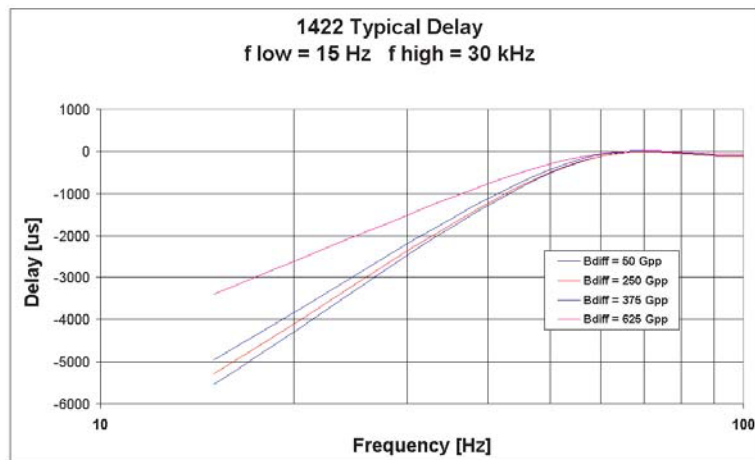
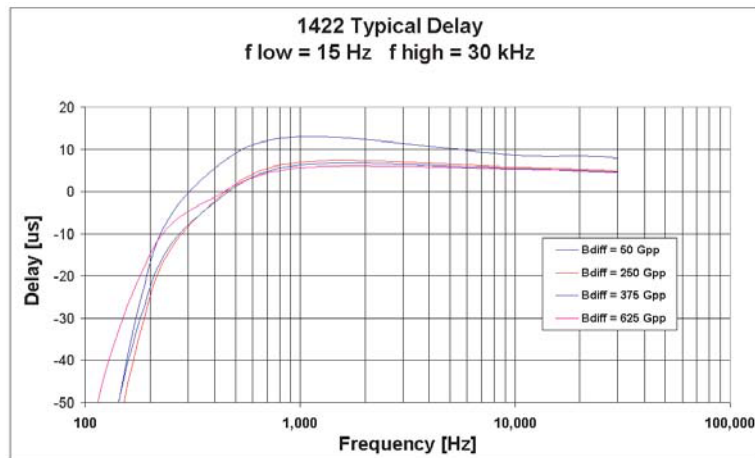
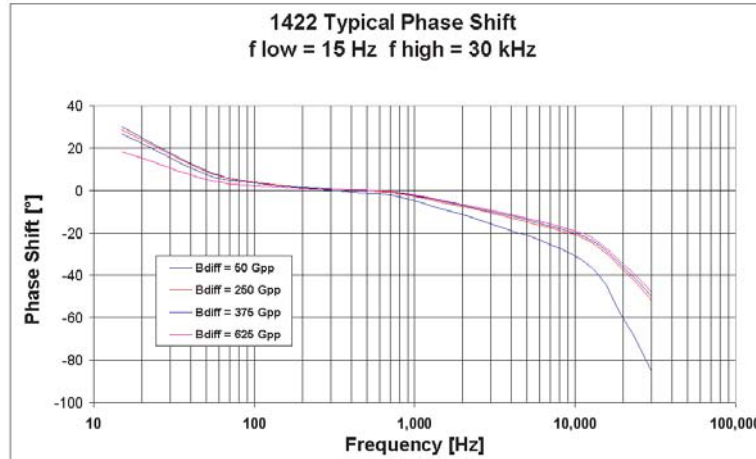


### Simulation Results, continued



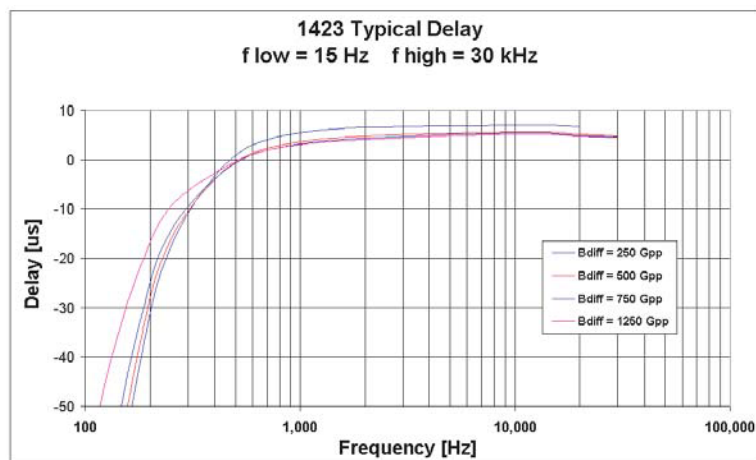
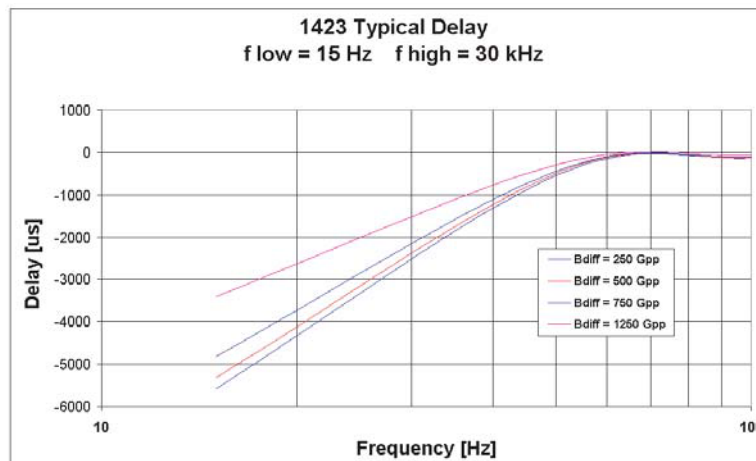
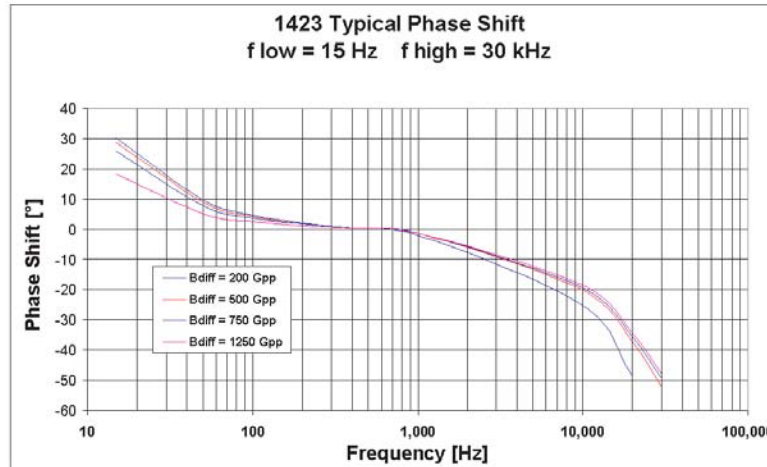
Continued on next page.

### Simulation Results, continued



Continued on next page.

### Simulation Results, continued

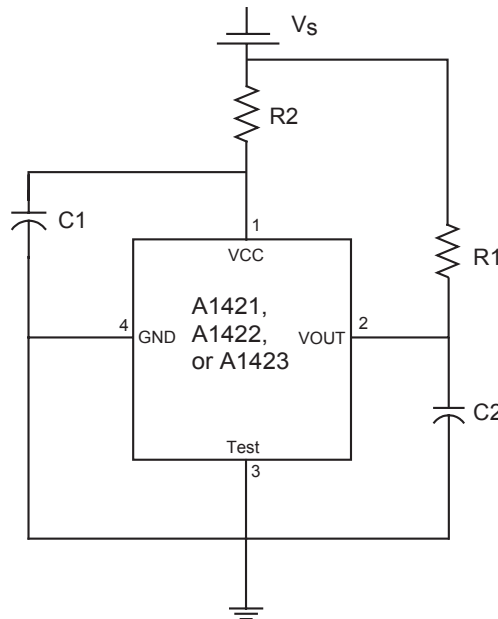


### Sensor Evaluation: EMC Characterization

Please contact Allegro MicroSystems for EMC performance information.  
(EMC test results are available after review of first silicon.)

Test Name	Reference Specification
ESD – Human Body Model*	AEC-Q100-002
ESD – Machine Model	AEC-Q100-003
Conducted Transients	ISO 7637-1
Direct RF Injection	ISO 11452-7
Bulk Current Injection	ISO 11452-4
TEM Cell	ISO 11452-3

\*ESD test is done with no external components.



Component	Value	Units
R1*	1	k $\Omega$
R2	100	$\Omega$
C1	0.1	$\mu$ F
C2	0.1	nF

\*Pull-up resistor not required for protection but for normal operation.

Recommended EMC test circuit. Test circuit recommended configuration may change after evaluation of first silicon.

### Applications Information

The A1421, A1422, and A1423 are versatile high-precision differential sensing devices that can be used in a wide range of applications. Proper choice of the target material and shape, magnet material and shape, and assembly techniques enables large working air gaps and high switchpoint accuracy over the device operating temperature range.

#### Sensor Operation

The device sensor IC contains two integrated Hall transducers that are used to differentially sense a magnetic field across the surface of the IC. Referring to figure 1, which shows curves for the A1421 as an example, the trigger switches the output when the differential magnetic field crosses the  $B_{OP}$  level while increasing in strength (referred to as the positive direction). In the example, the A1421 output voltage switches high (off), and switches the output low (on) when the differential magnetic field crosses  $B_{RP}$  while decreasing (the negative direction).

The operation is achieved through the use of two separate comparators. One comparator has a positive hysteresis,  $B_{HYS1}$ , and

the other a negative hysteresis,  $B_{HYS2}$ . Therefore, one comparator switches at the  $B_{OP}$  crossing on an increasing differential signal and the other switches at the  $B_{RP}$  crossing on a decreasing differential signal. The hysteresis on each comparator precludes false switching on noise or target jitter.

The behavior is similar for the A1422 and the A1423. The switchpoints are as shown in the magnetic characteristics table, and the output polarity is inverted. This is illustrated in figure 2, on the next page.

#### Start-up

During power-on time,  $t_{PO}$ , the output signal,  $V_{OUT}$ , is high. Beyond this time, if the applied magnetic field,  $B_{diff}$ , is smaller than  $B_{HYS}$ , the switching state and  $V_{OUT}$  polarity are indeterminate.  $V_{OUT}$  will be valid for  $B_{diff} > B_{HYS}$ , after the additional settling time,  $t_s$ , has also elapsed.

#### Delay

The bandpass filter induces delay in the output signal,  $V_{OUT}$ , relative to the applied magnetic field,  $B_{diff}$ . Simulation data shown

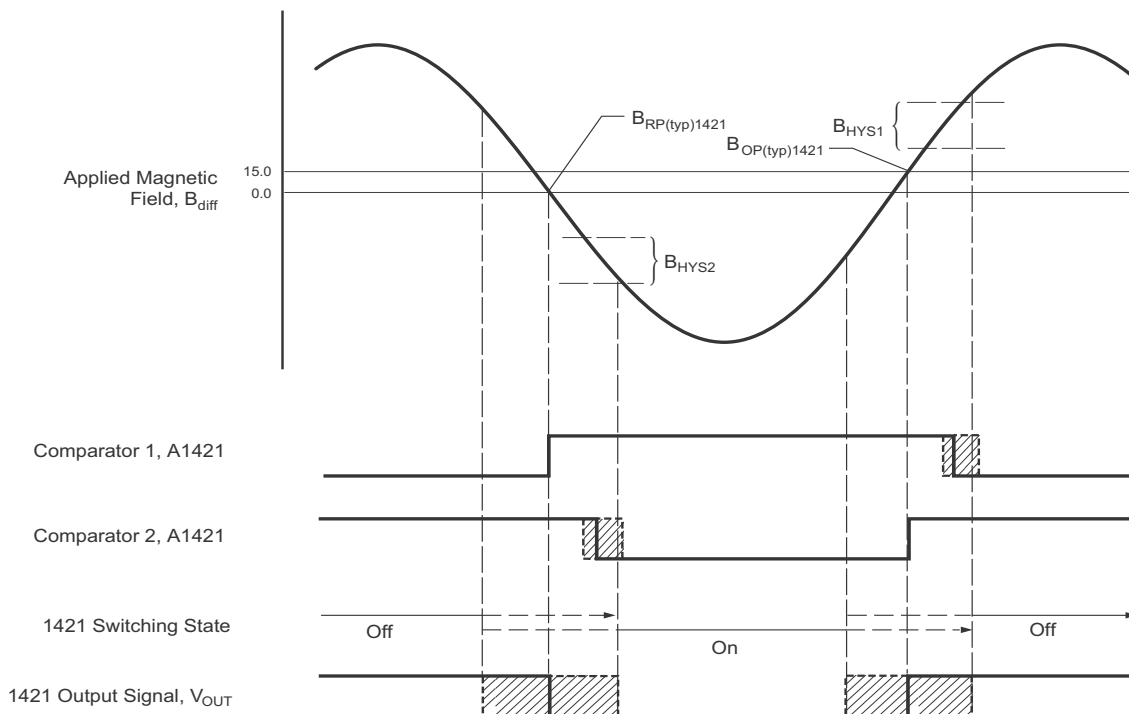


Figure 1. Typical output characteristics with dual comparator operation. The example shown is for the A1421. Characteristics shown without delay, see characteristic data charts for delay and phase shift contributions.

in the Characteristic Data section quantify the effect of the input signal amplitude on the phase shift of the output. Positive values of delay indicate a lagging output while negative values indicate a leading output.

### AC-Coupled Operation

Steady-state magnet and system offsets are eliminated using an on-chip differential bandpass filter. The upper and lower cut-off frequencies of this patented filter are set using an internal integrated capacitor. The differential structure of this filter improves the ability of the IC to reject single-ended noise on the GND or VCC line and, as a result, makes it more resistant to EMI (electromagnetic interference) typically seen in hostile remote-sensing environments.

### Power Supply Protection

The A1425 contains an on-chip voltage regulator and can operate over a wide supply voltage range. In applications that operate the device from an unregulated power supply, transient protection must be added externally. For applications using a regulated line, EMI/RFI protection may still be required. The circuit shown in figure 3 is the most basic configuration required for proper device operation.

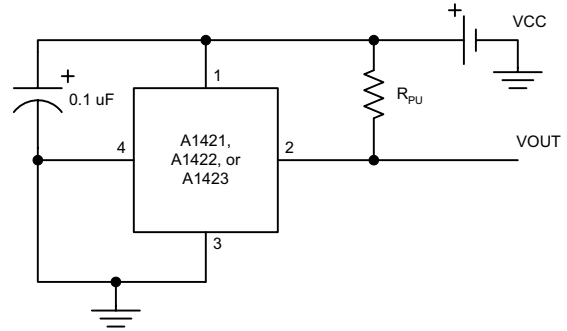


Figure 3. Basic application circuit. A pull-up resistor,  $R_{PU}$ , is required with the output driver.

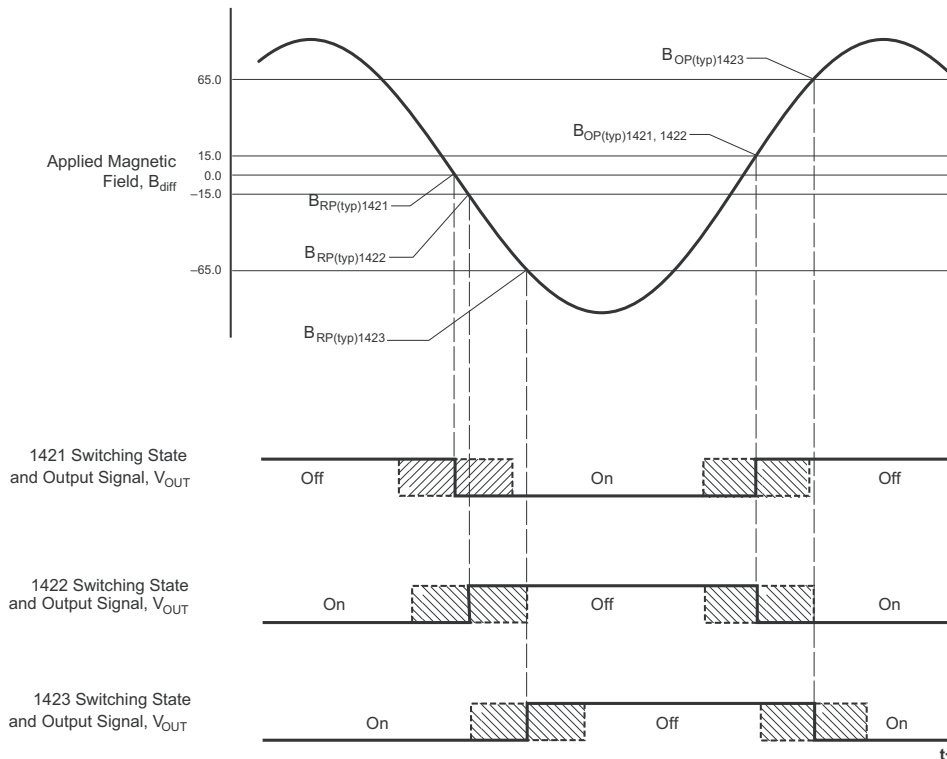


Figure 2. Comparative typical output characteristics. This chart illustrates the switchpoints and the output polarities of the A1421, A1422, and the A 1423. Characteristics shown without delay, see characteristic data charts for delay and phase shift contributions.

### Power Derating

The device must be operated below the maximum junction temperature of the device,  $T_{J(max)}$ . Under certain combinations of peak conditions, reliable operation may require derating supplied power or improving the heat dissipation properties of the application. This section presents a procedure for correlating factors affecting operating  $T_J$ . (Thermal data is also available on the Allegro MicroSystems Web site.)

The Package Thermal Resistance,  $R_{\theta JA}$ , is a figure of merit summarizing the ability of the application and the device to dissipate heat from the junction (die), through all paths to the ambient air. Its primary component is the Effective Thermal Conductivity,  $K$ , of the printed circuit board, including adjacent devices and traces. Radiation from the die through the device case,  $R_{\theta JC}$ , is relatively small component of  $R_{\theta JA}$ . Ambient air temperature,  $T_A$ , and air motion are significant external factors, damped by overmolding.

The effect of varying power levels (Power Dissipation,  $P_D$ ), can be estimated. The following formulas represent the fundamental relationships used to estimate  $T_J$ , at  $P_D$ .

$$P_D = V_{IN} \times I_{IN} \quad (1)$$

$$\Delta T = P_D \times R_{\theta JA} \quad (2)$$

$$T_J = T_A + \Delta T \quad (3)$$

For example, given common conditions such as:  $T_A = 25^\circ\text{C}$ ,  $V_{CC} = 12\text{ V}$ ,  $I_{CC} = 4.2\text{ mA}$ , and  $R_{\theta JA} = 177\text{ }^\circ\text{C/W}$ , then:

$$P_D = V_{CC} \times I_{CC} = 12\text{ V} \times 4.2\text{ mA} = 50\text{ mW}$$

$$\Delta T = P_D \times R_{\theta JA} = 50\text{ mW} \times 177\text{ }^\circ\text{C/W} = 9^\circ\text{C}$$

$$T_J = T_A + \Delta T = 25^\circ\text{C} + 9^\circ\text{C} = 34^\circ\text{C}$$

A worst-case estimate,  $P_{D(max)}$ , represents the maximum allowable power level ( $V_{CC(max)}$ ,  $I_{CC(max)}$ ), without exceeding  $T_{J(max)}$ , at a selected  $R_{\theta JA}$  and  $T_A$ .

### Example

Reliability for  $V_{CC}$  at  $T_A = 150^\circ\text{C}$ , package L-11, using minimum-K PCB

Observe the worst-case ratings for the device, specifically:  $R_{\theta JA} = 177^\circ\text{C/W}$ ,  $T_{J(max)} = 165^\circ\text{C}$ ,  $V_{CC(max)} = 26.5\text{ V}$ , and  $I_{CC(max)} = 7.0\text{ mA}$ .

Calculate the maximum allowable power level,  $P_{D(max)}$ . First, invert equation 3:

$$\Delta T_{max} = T_{J(max)} - T_A = 165^\circ\text{C} - 150^\circ\text{C} = 15^\circ\text{C}$$

This provides the allowable increase to  $T_J$  resulting from internal power dissipation. Then, invert equation 2:

$$P_{D(max)} = \Delta T_{max} \div R_{\theta JA} = 15^\circ\text{C} \div 177\text{ }^\circ\text{C/W} = 91\text{ mW}$$

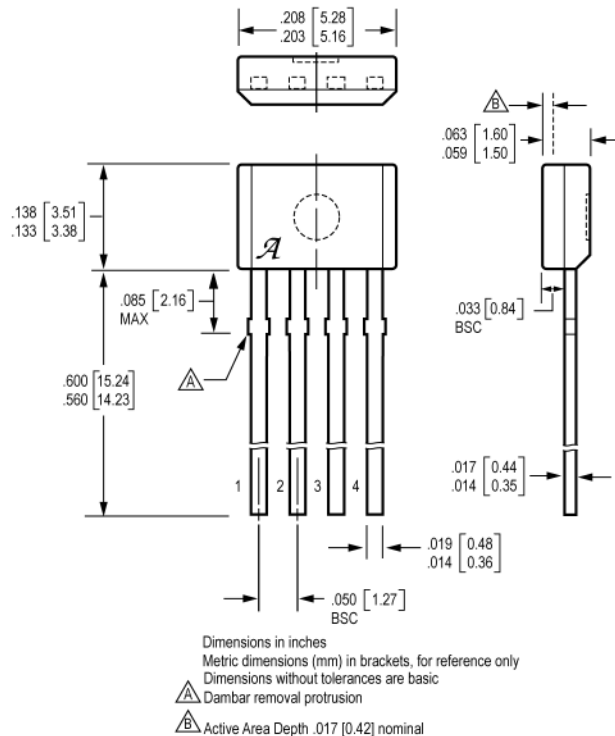
Finally, invert equation 1 with respect to voltage:

$$V_{CC(est)} = P_{D(max)} \div I_{CC(max)} = 91\text{ mW} \div 7.0\text{ mA} = 13\text{ V}$$

The result indicates that, at  $T_A$ , the application and device can dissipate adequate amounts of heat at voltages  $\leq V_{CC(est)}$ .

Compare  $V_{CC(est)}$  to  $V_{CC(max)}$ . If  $V_{CC(est)} \leq V_{CC(max)}$ , then reliable operation between  $V_{CC(est)}$  and  $V_{CC(max)}$  requires enhanced  $R_{\theta JA}$ . If  $V_{CC(est)} \geq V_{CC(max)}$ , then operation between  $V_{CC(est)}$  and  $V_{CC(max)}$  is reliable under these conditions.

### Package K, 4-pin SIP



The products described herein are manufactured under one or more of the following U.S. patents: 5,045,920; 5,264,783; 5,442,283; 5,389,889; 5,581,179; 5,517,112; 5,619,137; 5,621,319; 5,650,719; 5,686,894; 5,694,038; 5,729,130; 5,917,320; and other patents pending.

Allegro MicroSystems, Inc. reserves the right to make, from time to time, such departures from the detail specifications as may be required to permit improvements in the performance, reliability, or manufacturability of its products. Before placing an order, the user is cautioned to verify that the information being relied upon is current.

Allegro products are not authorized for use as critical components in life-support devices or systems without express written approval.

The information included herein is believed to be accurate and reliable. However, Allegro MicroSystems, Inc. assumes no responsibility for its use; nor for any infringement of patents or other rights of third parties which may result from its use.

Copyright © 2004 Allegro MicroSystems, Inc.